CrossMark

ORIGINAL PAPER

The impact of global warming on Kuroshio Extension and its southern recirculation using CMIP5 experiments with a high-resolution climate model MIROC4h

Xing Zhang[1,2] · Qiang Wang[1,3] · Mu Mu[1,3]

Abstract Responses of the Kuroshio Extension (KE) and its southern recirculation gyre (SRG) to global warming are investigated using CMIP5 experiments with a high-resolution climate model MIROC4h. The results show that MIROC4h well reproduces the essential features of the KE system and its low-frequency variations. In three-member-ensemble future climate experiments (with a medium mitigation emissions scenario RCP4.5), the strengths of the KE and its SRG increase, relative to the prescribed historical run with natural and anthropogenic forcing. By investigating the mechanism resulting in these variations of the KE and its SRG, it turns out that wind stress changes and ocean stratification changes both contribute to the enhancement of the KE and its SRG. Specifically, the wind stress changes increase upper ocean momentum in the SRG region. Meanwhile, the increased stratifications hinder the transfer of momentum from the upper ocean to the deeper ocean. Besides, the strengthened ocean stratification could enhance the eddy kinetic energy (EKE) in the downstream KE region, which can feedback to intensify the SRG. As a result, the strength of the SRG increases under global warming condition. Then the intensification of the SRG leads to large acceleration of the KE. Eventually, both the KE and its SRG intensify.

✉ Qiang Wang
wangqiang@qdio.ac.cn

1 Key Laboratory of Ocean Circulation and Waves, Institute of Oceanology, Chinese Academy of Sciences, Qingdao 266071, China

2 University of Chinese Academy of Sciences, Beijing 100049, China

3 Function Laboratory for Ocean Dynamics and Climate, Qingdao National Laboratory for Marine Science and Technology, Qingdao 266071, China

1 Introduction

The Kuroshio Extension (KE) is an eastward inertial jet in the mid-latitude North Pacific and forms after the Kuroshio separating from the Japanese coast at around (35°N, 141°E). Accompanying with the KE, a recirculation gyre tightly flanks on its south. Qiu and Chen (2005) pointed out that the transport of the southern recirculation gyre (SRG) is closely associated with the states of the KE and thus the KE and its SRG are recognized as a whole system.

Based on satellite altimeter measurements and eddy-resolving ocean general circulation models, some studies show that the KE system exhibits clearly decadal modulations between stable and unstable states (e.g., Qiu and Chen 2005, 2010; Taguchi et al. 2007, 2010; Kelly et al. 2010; Ceballos et al. 2009; Qiu et al. 2014). Notice that, following Qiu et al. (2014), we use terminology "stable" and "unstable" in this study to represent the dynamic state of the KE system; it is not in reference to the necessary condition for instability of the KE. The dynamic mechanisms for the transitions between the stable and unstable states have been explored (Miller et al. 1998; Schneider et al. 2002; Qiu 2003; Taguchi et al. 2007; Sasaki et al. 2013), and the results show that the transitions are mainly controlled by the low-frequency oscillation of the wind stress forcing over the central North Pacific Ocean.

The variations of the KE and its SRG have a significant impact not only on local climate but also on the global climate through air-sea interaction (e.g., Qiu 2002; Kwon et al. 2010; Frankignoul et al. 2011). Hence, the studies about the KE and its SRG have attracted the attention of many researchers. According to Waterman and Jayne (2009), the formation mechanisms for the SRG can be divided into three categories: the eddy-driven theory (Cessi 1988; Berloff 2005; Qiu et al. 2008), the inertial theory (Marshall and Nurser 1986; Marshall and Marshall 1992; Cessi 1988), and the unstable jet theory

(Jayne et al. 1996; Beliakova 1998; Jayne and Hogg 1999). The SRG can be affected significantly by changing the external forcing and the dissipation and the stratification in numerical experiments (Liu 1997; Chang et al. 2001; Qiu and Miao 2000; Pierini et al. 2009; Dijkstra 2000; Dijkstra and Ghil 2005; Sun et al. 2013).

Over the past 100 years, the global average temperature has increased by approximately 0.6 °C (Houghton et al. 2001). Previous studies found that sea surface temperature over the western boundary current of Northern Hemisphere has significantly increased over the last 25 years (Susan et al. 2007; Guan and Nigam 2008). Thus, it is interesting to investigate how the KE and its SRG respond to global warming condition. The analysis of the effects of warming condition on the KE system region will not only help us to predict the regional climate around Japan but also give us a better understanding of the global climate changes in the future.

Despite of the importance of the KE and its SRG, few studies focus on KE system responses to global warming. In the past, coarse-resolution ocean models ($1° \times 1°$ or coarser) have been used in the projections of climate change by global atmosphere-ocean coupled general circulation models (CGCMs). In coarse-resolution ocean models, the KE cannot be simulated well, and the latitude of the Kuroshio separation overshoots to the north when compared with observation (Choi et al. 2002). Such coarse-resolution ocean models are not suitable to investigate the changes of the KE and its SRG under global warming scene. Therefore, developing high-resolution coupled models is the key point to pursue this issue. High-resolution simulations with a coupled ocean-atmospheric model MIROC3.2 provide the first view on the response of the KE system to global warming, with atmospheric CO_2 concentration ideally increasing by 1 % per year (Sakamoto et al. 2005). Their analytical results suggest that the increased atmospheric CO_2 concentration would cause an acceleration of the KE current as a result of the SRG spin-up. They regarded the spin-up of the SRG as a result of the combined effects of local wind stress changes and the nonlinear formation mechanisms (Taguchi et al. 2005) induced by the acceleration of the Kuroshio. However, they did not consider the effects of changes in sea water properties (e.g., temperature, salinity, stratification). As some studies have examined, the sea water properties have significantly changed under global warming condition (Cravatte et al. 2009; Deser et al. 2010; Capotondi et al. 2012). Whether these changes may contribute to variations of the KE system needs to be clarified.

Based on the above considerations, the present study will investigate the responses of the KE and its SRG to global warming and reveal the response mechanisms. Specially, we try to clarify whether wind stress change is the only factor that intensifies the KE system or sea water properties change also contributes to the enhancement of the KE system. Here we use the datasets of a high-resolution climate model MIROC4h (the improved model that Sakamoto et al. 2005 used in their study) from Coupled Model Intercomparison Project Phase 5 (CMIP5) experiments. MIROC4h has the highest atmosphere resolutions (0.5625° zonally and 0.5625° meridionally) and ocean resolutions (so-called eddy-permitting horizontal resolution 0.28125° zonally and 0.1875° meridionally) in the climate models used in CMIP5. With a similar resolution, a much simpler ocean model could provide significant modeling of the KE low-frequency variability (Pierini 2006), and the KE can be resolved enough in this resolution.

The rest of the paper is organized as follows. Section 2 describes the MIROC4h model and the experimental procedure. Section 3 examines the simulation ability of the MIROC4h to the mean state and the low-frequency variability of the KE system. The responses of the KE and its SRG to global warming are investigated in Section 4. Section 5 discusses the detailed mechanisms of the responses. The summary and discussion is given in Section 6.

2 Model description and the experimental procedure

MIROC4h is cooperatively developed by the Atmosphere and Ocean Research Institute of the University of Tokyo, National Institute for Environmental Studies (NIES) and Japan Agency for Marine-Earth Science and Technology. MIROC4h consists of five model components simulating atmosphere, land surface, river-routing, ocean, and sea ice subsystems, respectively.

The atmospheric component model in MIROC4h is based on a global spectral dynamical core and a standard physics package (K-1 Model Developers 2004) developed at the Center for Climate System Research (CCSR)/NIES/Frontier Research Center for Global Change (FRCGC). The horizontal resolution of the atmospheric component is 0.5625°, which is twice the resolution for the previous generation model MIROC3h. Vertically, the sigma (pressure normalized by the surface pressure) coordinate system is adopted, and this atmospheric component model has 56 σ-layers with a relatively fine vertical resolution near the planetary boundary.

The ocean general circulation model in MIROC4h is the CCSR ocean model (Hasumi 2006) which includes a sea ice model (K-1 Model Developers 2004; Komuro et al. 2012). The spherical coordinate system used in this model involves a rotated grid in order to avoid a singular point in the ordinary latitude-longitude coordinates at the North Pole. The horizontal resolution is 0.28125° zonally and 0.1875° meridionally. The number of vertical levels excluding the bottom boundary layer is 47. The time step of the model integration is 3 s for the barotropic mode and 3 min for the others. No correction is applied in exchanging water, heat, and momentum fluxes between the ocean and the atmosphere. In addition, a land model

that incorporates a river module is used (Takata et al. 2003; K-1 Model Developers 2004).

Sakamoto et al. (2012) investigated the simulation of MIROC4h and they found that many improvements have been achieved when compared with MIROC3h: errors in the surface air temperature and sea surface temperature are reduced; temperature in the deep ocean becomes more realistic; coastal upwelling motion in the ocean has been improved; drift of the orographic wind and its effects on the ocean become less.

MIROC4h has been used to carry out the historical and future climate simulations. The procedure is as follows. Firstly, an output of 100 years (1850–1950) pre-industrial (piControl) simulation was supplied with fixed external forcing (e.g., greenhouse gases, aerosols concentrations, ozone, solar irradiance) at the 1950 level. After the piControl simulation, three-ensemble twentieth century climate simulations (refer to historical ensemble, 1951–2005) were carried out. All the three-ensemble historical simulations (hereafter, H1, H2, and H3) were forced by time-varying natural and anthropogenic forcing (e.g., greenhouse gases, aerosol concentrations, ozone, solar irradiance) taken from observations (1951–2005). Although under the same forcing conditions, the three-ensemble historical simulations were started from three different initial states obtained from three arbitrary points in the piControl simulation (Taylor et al. 2012). The three-ensemble historical simulations were extended to the year 2035 with future emission scenarios as the subsequent future climate simulations (hereafter, R1, R2, and R3). In the future climate simulations, the climate model is forced by a medium mitigation emissions scenario RCP4.5. RCP4.5 identifies a concentration pathway that approximately results in an additional radiative forcing of 4.5 W m^{-2} at year 2100, relative to pre-industrial conditions. It is a stabilization scenario where total radiative forcing is stabilized before 2100 by employment of a range of technologies and strategies for reducing greenhouse gas emissions (Moss et al. 2008, 2010). The scenario drivers and technology options are detailed in Clarke et al. (2007).

It is worth noting that the three-ensemble simulations were started from three different initial conditions obtained from three different points in the piControl simulation rather than realistic atmosphere-ocean initial conditions. Because the internally generated climate variability is sensitive dependent on initial conditions, each simulation member has a different phase of internally generated climate variability. In this situation, the internally generated climate variability in the three-ensemble simulations will only by coincidence match the realistic situation (Taylor et al. 2012). Therefore, the "year" mentioned in the historical and future climate simulations is "model year," which represents the running time of the model. Within a certain model year, the responses of ocean and atmosphere are different from each other in the three-ensemble

simulations of MIROC4h and could not correspond to the reality in the corresponding actual year.

In short, MIROC4h conducts three-ensemble simulations (Simulation-1, Simulation-2, and Simulation-3) including historical simulations (H1, H2, and H3) for the periods 1951–2005 using the historical forcing dataset and subsequent three-member ensemble future climate simulations (R1, R2, and R3) for the periods 2006–2035 with a medium mitigation emissions scenario RCP4.5 in CMIP5 experiments.

3 Simulation of the KE and its SRG in MIROC4h

Before investigating the responses of the KE and its SRG to global warming, the simulation capability of MIROC4h to the KE system should be examined first.

Figure 1a shows the standard deviation of interannual sea surface height (SSH) variations (shaded) and the absolute mean SSH fields (contour) of H1. The calculation of the standard deviation is based on monthly anomalies defined as deviations from the 55 model years (1951–2005) monthly mean climatology. Because we mainly focus on the interannual to decadal variations of KE and its SRG, a 12-month low-pass filter is employed to remove seasonal and higher-frequency oscillations. In this situation, mesoscale eddies might be suppressed. The figure shows that the MIROC4h model captures the essential features of both the mean and interannual variations of the KE system. A sharp KE front is found at around 34°–37°N with two well-developed quasi-stationary meanders east of Japan in the KE at 144°E and 150°E. The SRG is flanked on south of the KE front around 31°–35°N. High interannual variations are concentrated within a narrow latitudinal band along the mean KE front. Specifically, near (35°N, 144°E), the standard deviation exceeds 36 cm within a frontal band, while in the most regions outside of the band, the standard deviation is less than 15 cm. The same conclusion can also be obtained from H2 and H3 (Fig. 1b, c). The above spatial patterns are similar with the observational results and numerical simulation results shown by previous study (Taguchi et al. 2007).

The spatial and temporal structures of the low-frequency variations of the KE are also examined. Figure 2a shows the KE paths in the model years 1982–1987 of H1 as Qiu and Chen (2005) did. Here, the paths are defined by the 25-cm SSH contours. We also compare this indicator with the other indicators defined by the maxima temperature gradient or the max surface transport and find the results are similar. Figure 2a demonstrates that the KE paths are much more stable in the model years 1982–1984 than those in the model years 1985–1987. Figure 2b shows the KE paths defined by the 100-cm SSH contours in the actual years 2003–2008 from the satellite altimeter measurements. Comparing the Fig. 2a, b, we find that the KE states in the model years 1982–1984 and
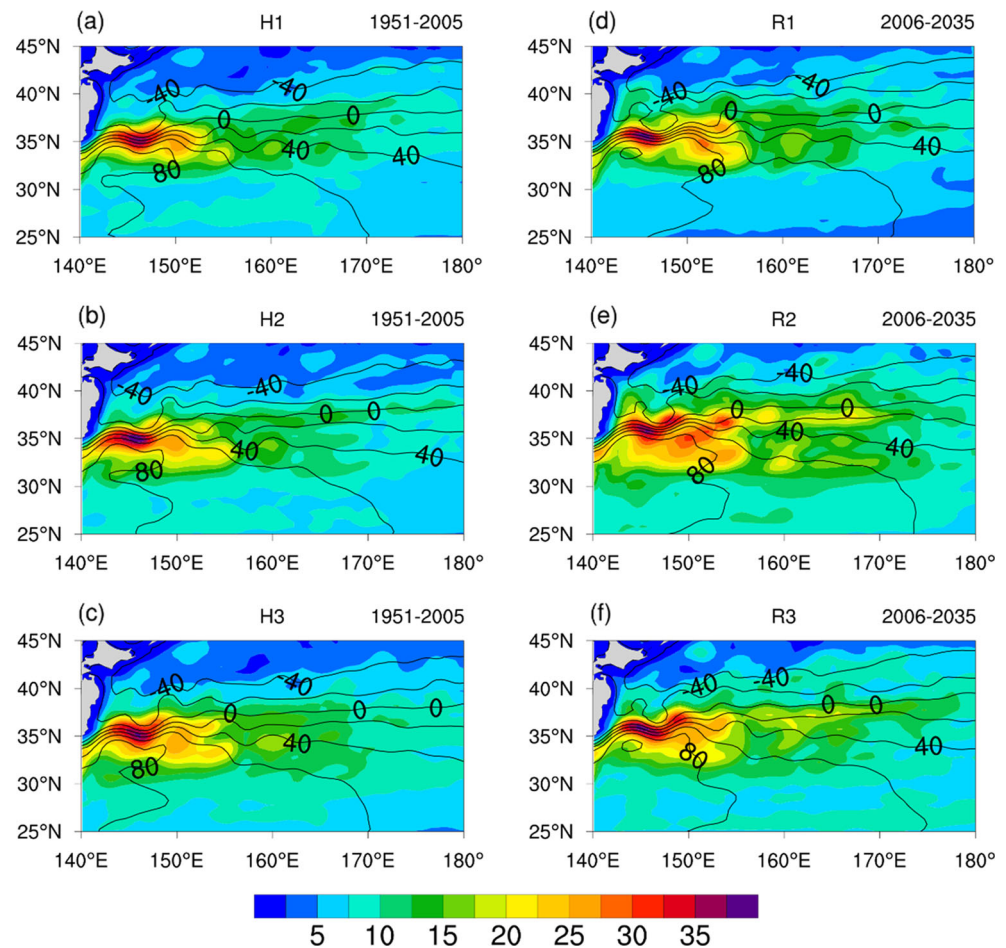
1985–1987 are very similar to the observed stable and unstable states in the actual years 2003–2005 and 2006–2008. This reflects that MIROC4h appears to be able to simulate the two different states of the KE system. It is worth noting that KE system is a complex nonlinear ocean system. In addition to responding to external forcing, the KE system exhibits low-frequency variations solely due to its self-sustained intrinsic relaxation oscillation (Pierini 2006). As mentioned in Section 2, the three-ensemble simulations were started from three different initial conditions obtained from three different points in the piControl simulation rather than realistic atmosphere-ocean initial conditions. In this situation, the KE low-frequency variations in the historical simulations will only by coincidence match the realistic situation because the nonlinear KE system is sensitive dependent on initial conditions. This is the reason why we compare the modeled monthly paths in the model years 1982–1987 with the observed monthly paths in the actual years 2003–2008.

In order to quantify the variations of the KE system in MIROC4h, the time series of the upstream KE path length (L-KE) is calculated. L-KE was introduced by Qiu and Chen (2005) and has been proved to be an extremely efficient indicator to characterize the KE system low-frequency variations

(Pierini 2015). Here the L-KE is defined as the upstream KE path length integrated from 141° to 153°E as Qiu and Chen (2005) did. Figure 3 shows the time series of the L-KE in three-ensemble simulations. It is clear from the time series that MIROC4h has the ability to simulate the two distinct states of the KE system. When the KE system is in the stable state (e.g., in the model years 1982–1984 of H1), the KE paths are elongated and the L-KE is at a relatively low level (about 2000 km, black line) accompanied by weak temporal variability. However, when the KE system switches to an unstable state (e.g., in the model years 1985–1987 of H1), the KE paths become much more convoluted and exhibit monthly time-scale fluctuations resulting from the shedding and merging of mesoscale eddies. In the meantime, the L-KE reaches to a relatively high level (about 3000 km, black line) accompanied by strong temporal variability. These phenomena are in agreement with observations (Qiu and Chen 2005; Qiu et al. 2014). Then we investigate the KE system transforms from one state to another through spectrum analysis of the time series of L-KE and find that the period is about 14 years, which is similar with the observation fact (Qiu 2003). We also examine the dynamic mechanisms for the transitions between the stable and unstable states of the KE system in MIROC4h. Figure 4

Fig. 2 **a** Monthly paths of the Kuroshio Extension derived from sea surface height above geoid of MIROC4h historical simulation (H1) in the model years 1982–1987. The paths are defined by the 25-cm surface height above geoid. **b** Monthly paths of the Kuroshio Extension defined by the 100-cm contours in the SSH fields in the years 2003–2008 from the satellite altimeter measurements
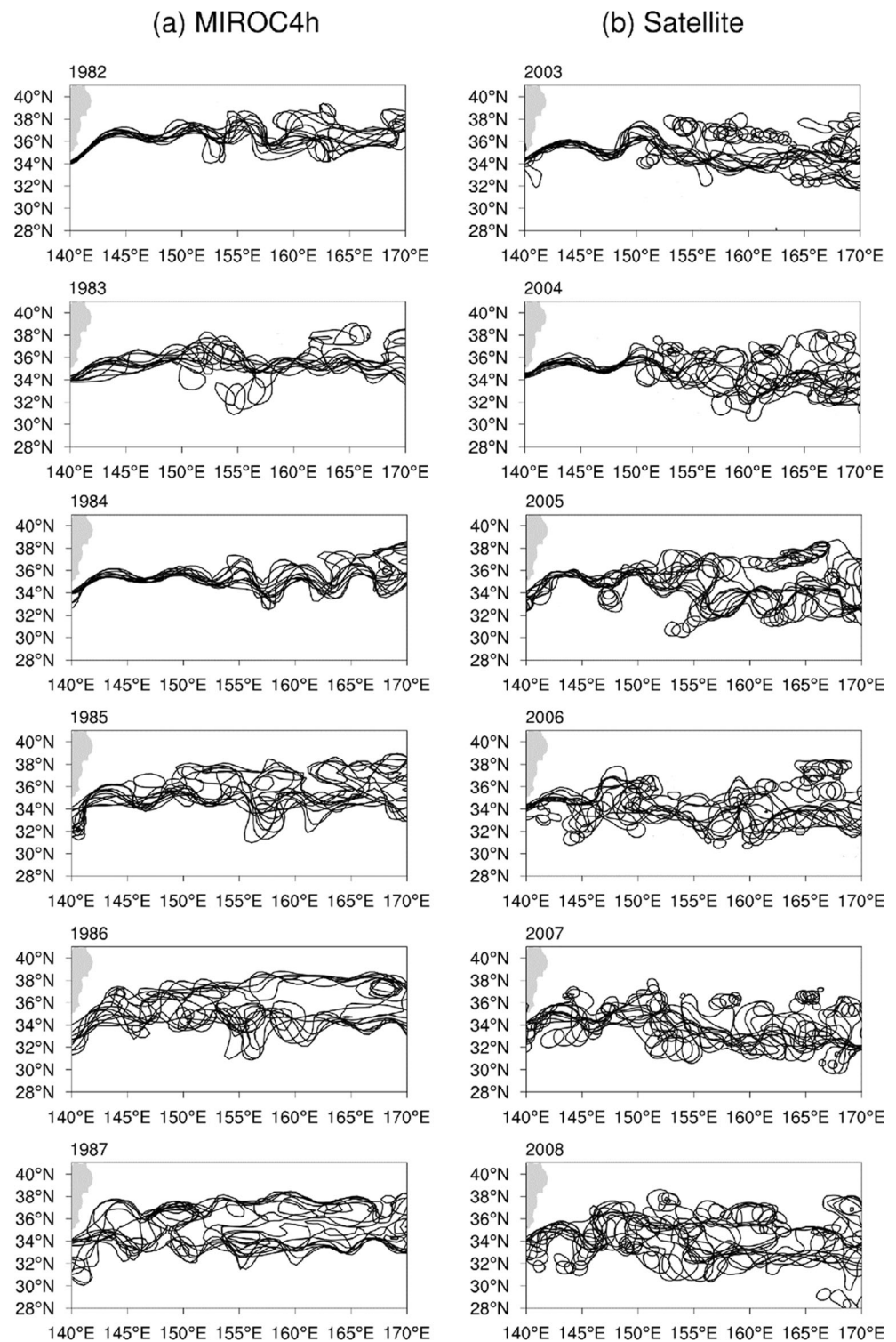
shows the monthly SSH anomalies averaged over the latitudinal band of the KE (34°–37°N) as a function of time and longitude in model years 1960–1990 of H1. As shown in the Fig. 4, although there exist some noises due to the presence of the mesoscale eddy variabilities, the SSH anomalies signals, especially those associated with the interannual variations,

have a consistent pattern: SSH anomalies first appear in the downstream KE region and then propagate westward (see the solid lines). When these positive (negative) SSH anomalies arrive in the KE region, they lead to a stable (unstable) state of the KE system. This confirms that in the MIROC4h model, the remotely forced SSH anomalies play a modulating role in

Fig. 3 The time series of the upstream KE path length for the three historical simulations. The vertical coordinate means the path length; unit, km
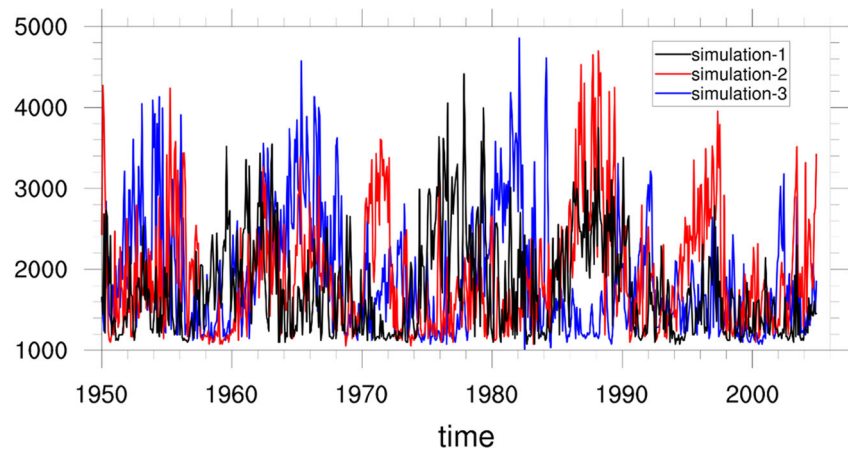
the transitions of KE system as shown by previous studies (Qiu 2003; Qiu et al. 2014).

The above results imply that the MIROC4h model well reproduces the essential features of the KE system and its low-frequency variations. Hence, the MIROC4h datasets in CMIP5 experiments will be used to investigate the responses of the KE and its SRG to global warming.

4 The responses of the KE and its SRG to global warming

In this section, we will illustrate the responses of the KE and its SRG to global warming by comparing three-ensemble historical simulations with three future emission scenarios simulations. Because the MIROC4h model only provides future

Fig. 4 Time-longitude plots of SSH anomalies averaged between 34°N and 37°N in model years 1960–1990 for MIROC4h historical simulation (H1)

climate experiments with a period of 30 years while the period of the low-frequency variations of the KE system is about 14 years, it is difficult for us to statistically confirm whether the occurrence frequency of the stable or unstable states of the KE system has significant change under global warming. Hence, we mainly focus on the changes of the mean state of KE system caused by warming. Notice that Sakamoto et al. (2005) used only one control-run experiment with one CO_2-run experiment in their study while we analyze three ensemble simulations in the present study.

Similar to Fig. 1a, Fig. 1d shows the standard deviation of interannual SSH variations (shaded) and the absolute mean SSH fields (contour) of R1. The calculation of the standard deviation is based on monthly anomalies defined as deviations from the 30 model years (2006–2035) monthly climatology. In R1, the strengths of the KE and its SRG to the west of 150°E apparently increase in comparison with H1. In H1, the SRG has a maximal SSH less than 100 cm while the maximal SSH is over 100 cm near (145°E, 34°N) in R1. Comparing the 80-cm contour lines between H1 and R1, the SRG in R1 has a higher SSH than that in H1, which means that the SRG intensifies in warming scene. The other two simulations show the same results (compare Fig. 1b, c with Fig. 1e–f).

In order to further quantify the intensification of the SRG, we calculate the time series of the SRG strengths of three simulations (the periods 1951–2005 for historical simulations and 2006–2035 for future climate simulations). Following Qiu and Chen (2005), the SRG strength is defined as follows:

$$S(t) = \iint_A h(x,y,t)dxdy \qquad (1)$$

where $h(x,y,t)$ is the SSH and A denotes the SRG region within which the SSH value exceeds a threshold h_o in the KE system region (30°–37°N, 141°–158°E). A value of h_o is chosen to be 50 cm for MIROC4h, which well represents the boundary of the SRG. The results are robust to the choice of the specific values of h_o between 50 and 80 cm. As Fig. 5
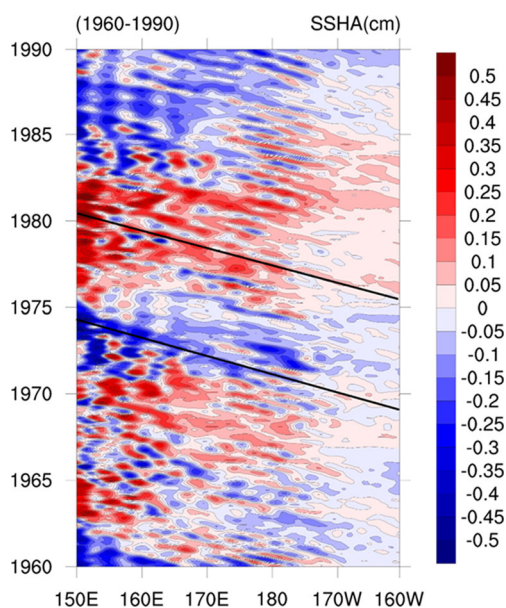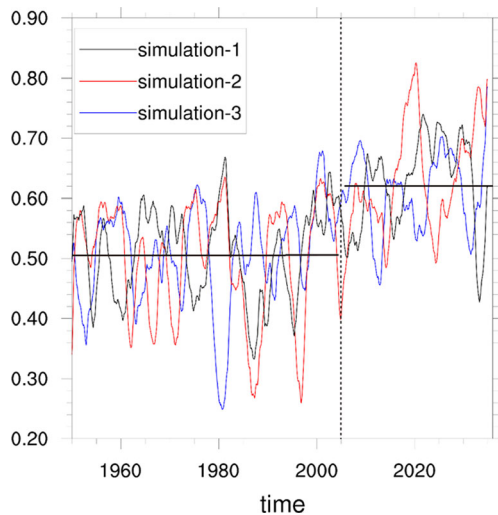
Fig. 5 The time series of the SRG strength for three MIROC4h ensemble simulations (the periods 1951–2005 for historical simulations and 2006–2035 for future climate simulations). The vertical coordinate means the strength; unit, cm. The *horizontal black lines* in the figure represent average values of each period for ensemble means from the three simulations. A 12-month low-pass filter is employed to remove seasonal and higher-frequency oscillations

shows, the strength of the SRG increases in all three future emission scenarios simulations. The average strength of the SRG intensifies from 0.509 m in H1 to 0.623 m in R1, from 0.499 m in H2 to 0.629 m in R2, and from 0.507 m in H3 to 0.609 m in R3. These changes all pass the *T*-tests at a significance level of 0.05. Of course, the internal variability may affect the results mentioned above. To remove the effects, we calculate ensemble means averaged from the three simulations, which are shown in Fig. 5 (see the horizontal black lines line). The results for the ensemble means also illustrate the strengthening of the SRG.

As mentioned in Section 1, the strength of the SRG is closely associated with the states of the KE system and this close connection is also reflected in MIROC4h. For instance, the KE system switches from stable state to unstable state in the model years 1982–1987 of H1; correspondingly, the strength of the SRG yields a strong decrease during this period (Fig. 5, black line). Comparing the L-KE with the SRG strength (compare Fig. 3 with Fig. 5), we find that the time series of the L-KE shows a strong negative correlation with the time series of the SRG strength. When the KE system is in the stable state, it tends to have a low L-KE indicator and an enhanced SRG. When the KE system switches to an unstable state, the L-KE indictor increases and the strength of the SRG weakens. These results clearly show that the KE indeed has a close connection with its SRG in MIROC4h and this close connection is in agreement with observations (Qiu and Chen 2005; Qiu et al. 2014). Since the strength of the SRG is closely associated with KE, the intensification of the SRG may lead to changes of the KE. Thus, we calculate the mean current speed in the region (34°–37°N, 141°–153°E) where the KE current

speed is relatively large. The results show that the mean KE current speed increases by about 0.1 m s^{-1} in the surface (0.350 m s^{-1} in H1 and 0.455 m s^{-1} in R1). The current speed from the surface to 600 m depth increases by 30–40 % in future emission scenarios simulations. To clearly show the spatial structure of the changed KE and its SRG, we plot the difference of current velocity at 100 m between H1 and R1 (latter minus former) in Fig. 6 (vector). Apparently, the current speed of the KE jet and the SRG largely increases. The same conclusions could be obtained by comparing H2 with R2 or H3 with R3. These results turn out that the KE and its SRG indeed intensify under global warming condition.

5 Mechanisms discussion

In this section, we will discuss why the KE system intensifies under global warming. Since the KE system is an important part of western boundary current of a wind-driven ocean gyre, the spin-up of subtropical gyre by wind in the North Pacific is a possible cause. Figure 7a–c (vector) shows the changes of the large-scale wind stress field caused by global warming. It is found that there are consistent east wind anomalies at about 30∼40°N in the three simulations. This means the westerlies weaken. Therefore, the whole subtropical gyre may not spin up. To further investigate the variations of the subtropical gyre, we first calculate the differences of Sverdrup transport stream function calculated from wind stress between three ensemble historical simulations and three future emission scenarios simulations in the North Pacific. Figure 8a–c indicates that in most regions of the subtropical gyre, the Sverdrup transport decreases about 2 Sv (1 Sv=10^6 m^3) in all future emission scenarios simulations. Then we examine the difference in the stream function for the upper ocean induced by warming (Fig. 6, shaded) and find that there exist negative anomalies in the most subtropical region. These results confirm that the subtropical gyre does not intensify under global warming condition in MIROC4h.

Of course, the local wind stress changes may induce the enhancement of the SRG. Figure 7a–c indicates that there are negative changes in the wind stress curl over the central-to-western part of mid-latitude North Pacific to the east of the KE system region in all of the three simulations, although their strengths and locations are different from each other. According to Sverdrup theory, these negative wind-stress curl differences would enhance Sverdrup transport in the KE system region. Specifically, in the region averaged over 33°–37°N, 143°–158°E, the Sverdrup transport calculated from wind stress increases about 2 Sv in Simulation-1, about 8 Sv in Simulation-2, and about 4 Sv in Simulation-3

Fig. 6 The difference of the stream function of the current at 100 m (*color shading* unit, $m^2 s^{-1}$) between the ensemble historical simulation (H1) and future emission scenarios simulation (R1) (latter minus former) and the difference of the current velocities at 100 m (vectors; unit, $m s^{-1}$) between ensemble historical simulation (H1) and future emission scenarios simulation (R1) (latter minus former)
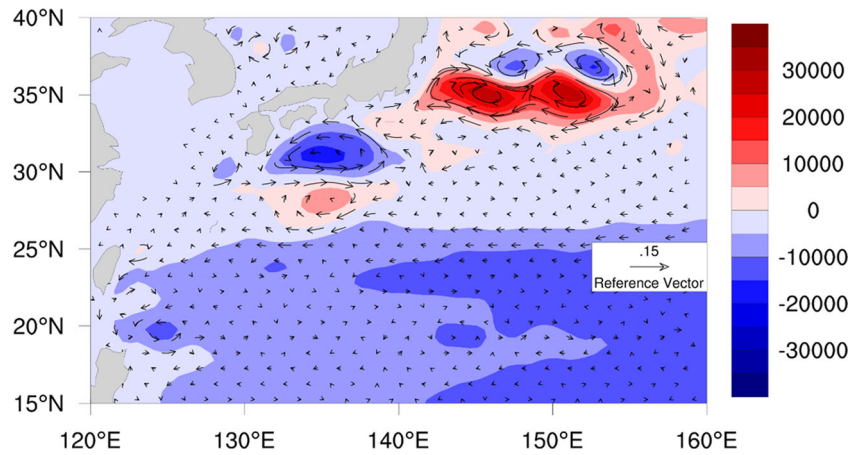
under global warming condition (Fig. 8a–c), which proves that the wind stress changes indeed contribute to the intension of the SRG to some extent. However, the vertically integrated volume transport increases about 25 Sv in this area in all three future emission scenarios simulations. Thus, the change in wind stress alone is not enough to explain the intensification of the

SRG under global warming condition. It should be noted that above results are similar with the findings of Sakamoto et al. (2005). In their study, the Sverdrup transport calculated from wind stress increases 5–6 Sv while the vertically integrated volume transport increases about 29 Sv in the SRG region under warming scene. Sakamoto et al. (2005) use the nonlinear
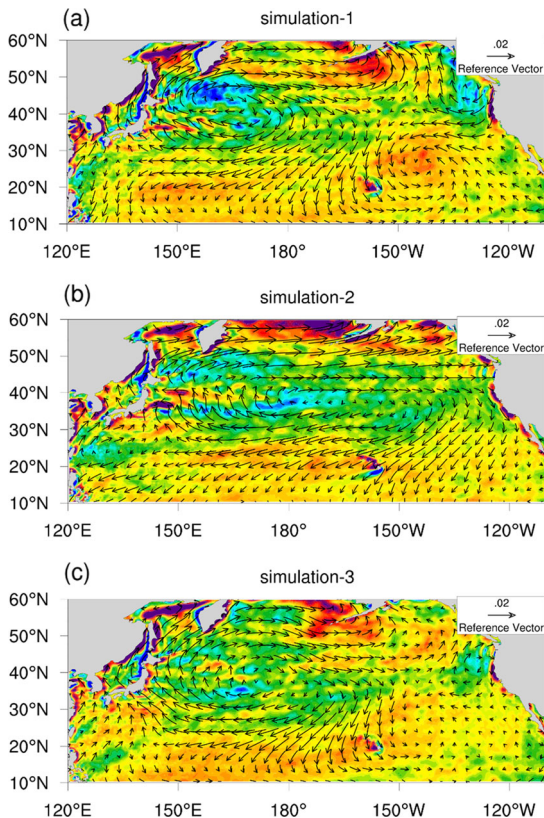

Fig. 7 a Differences of long-term mean wind stress (vectors; unit, $N m^{-2}$) and the curl (*color shading*; unit, $10^{-8} N m^{-3}$) between the ensemble historical simulation (H1) and future emission scenarios simulation (R1) (latter minus former). **b** As in (**a**), but for Simulation-2. **c** As in (**a**), but for Simulation-3
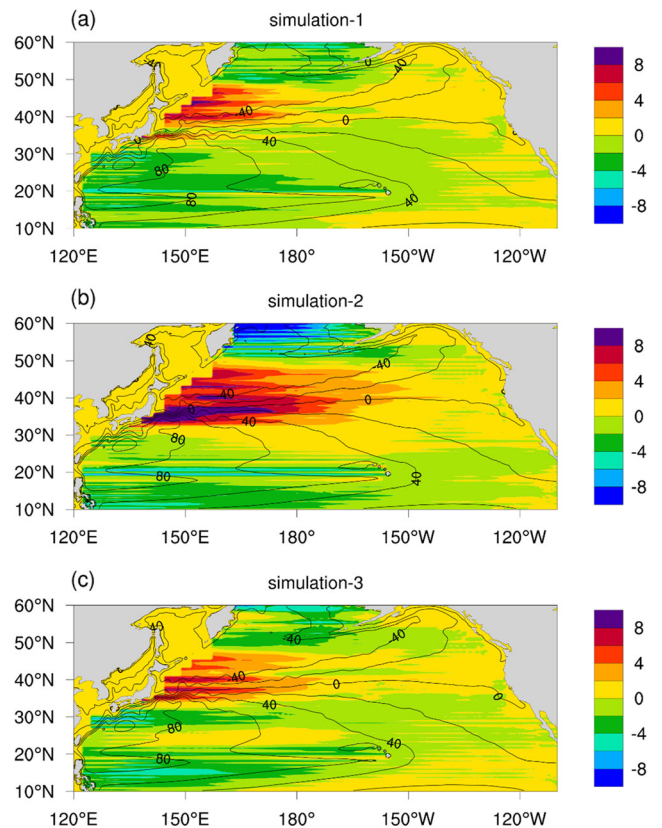

Fig. 8 a Differences of Sverdrup transport stream function (*color shading*; unit, $Sv = 10^6 m^3 s^{-1}$) between the ensemble historical simulation (H1) and future emission scenarios simulation (R1) (latter minus former) in the North Pacific and the mean sea surface height above geoid (contours at 20-cm intervals) of the ensemble historical simulation (H1). **b** As in (**a**), but for Simulation-2. **c** As in (**a**), but for Simulation-3

formation mechanisms to explain the discrepancy between the SRG response and the Sverdrup theory. However, as shown in Fig. 6, there is no evident increase in the current velocity of the Kuroshio, which means that there is no significantly enhancing advection of low potential vorticity (PV) water along the Kuroshio. Therefore, the nonlinear formation mechanisms cannot explain the enhancement of the SRG because the enhancing PV advection is a necessary part for the mechanism.

As mentioned in Section 1, in addition to the wind stress changes, the SRG can be affected by the ocean stratification changes. Naturally, we suspect whether the ocean stratification changes also contribute to the spin-up of the SRG in future emission scenarios simulations.

Firstly, we explore how the sea water properties of the KE system change in MIROC4h under global warming condition. Note that three simulations show the consistent results; for simplicity, we only indicate the results for Simulation-1 here. Figure 9a–d shows the differences of the temperature and salinity between the upper ocean and the deeper ocean in H1 and R1. The thermocline in the KE system region is about 700 m deep, so we choose 200 and 1000 m to represent the upper and deeper oceans, respectively. We find that the choice of the value to represent the upper ocean depth ranging from 1.5 to 400 m does not affect the following analysis results. Figure 9a, b indicates that the temperature differences in the SRG are about 12.2 K in H1 and increase to 13.2 K in R1. Figure 9c, d illustrates that the salinity differences in the SRG also increase under global warming. Further analysis finds that the increases of the temperature and salinity differences are mainly caused by the increase of temperature and salinity in the upper ocean. The increase of temperature would decrease the density, while the increase of salinity has the opposite effect in the upper ocean. Therefore, we need to investigate the relative influence of the temperature and salinity changes upon the density changes.

Following Capotondi et al. (2012), density changes are estimated as follows:

$$\Delta\rho = \rho\left(\overline{T_2}, \overline{S_2}\right) - \rho\left(\overline{T_1}, \overline{S_1}\right) \tag{2}$$

Here, overbars indicate time-averaged quantities; $\overline{S_1}$ and $\overline{T_1}$ are the average temperature and salinity in H1 (1951–2005), while $\overline{S_2}$ and $\overline{T_2}$ are the average temperature and salinity in R1 (2006–2035). The relative influences of the temperature and salinity changes upon the density changes are estimated as:

$$\Delta\rho_T = \rho\left(\overline{T_2}, \overline{S_1}\right) - \rho\left(\overline{T_1}, \overline{S_1}\right) \tag{3}$$

$$\Delta\rho_S = \rho\left(\overline{T_1}, \overline{S_2}\right) - \rho\left(\overline{T_1}, \overline{S_1}\right) \tag{4}$$

where $\Delta\rho_T$ and $\Delta\rho_S$ are the density changes due to the temperature and salinity changes, respectively. The approach outlined in Eqs. (3) and (4) is not exact, as the sum of Δp_T and Δp_S does not exactly match $\Delta\rho$, but the discrepancies are very small. Equations (3) and (4) provide a good estimate of the temperature and salinity contributions to the density changes (Capotondi et al. 2012). Figure 10a, b shows the contribution of the temperature and salinity changes to the potential density changes at 200 m. Apart from the small area in the northward of the KE around (147°E, 37°N) and (153°E, 37°N) where a hint of increased temperature and decreased salinity can be seen, the temperatures of the whole KE region enhance while the salinities reduce with the maximal value located in the KE jet and north of the SRG between a narrow latitude band over 34°–36°N extending from 141°E to 153°E. Besides, the

Fig. 9 a The temperature differences between 200 and 1000 m (former minus latter) in ensemble historical simulation (H1). **b** As in (**a**), but for future emission scenarios simulation (R1). **c** The salinity differences between 1000 and 200 m (former minus latter) in ensemble historical simulation (H1). **d** As for (**c**), but for future emission scenarios simulation (R1)
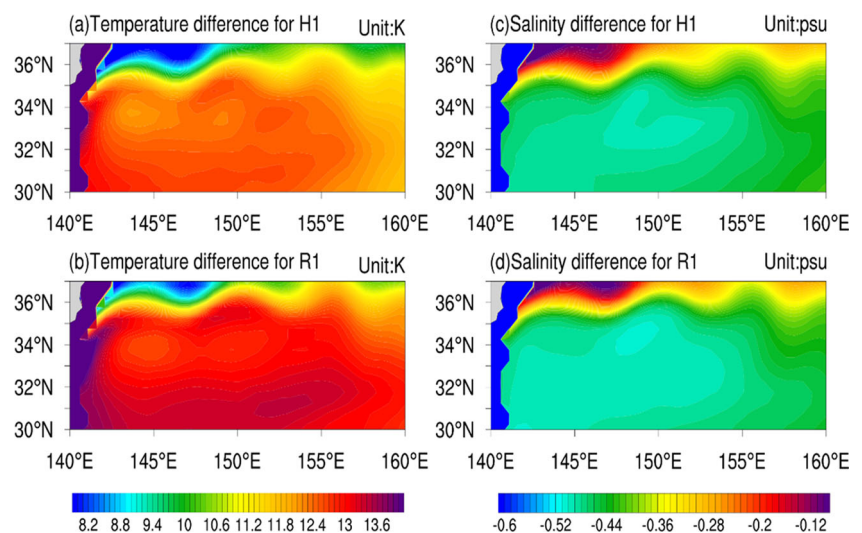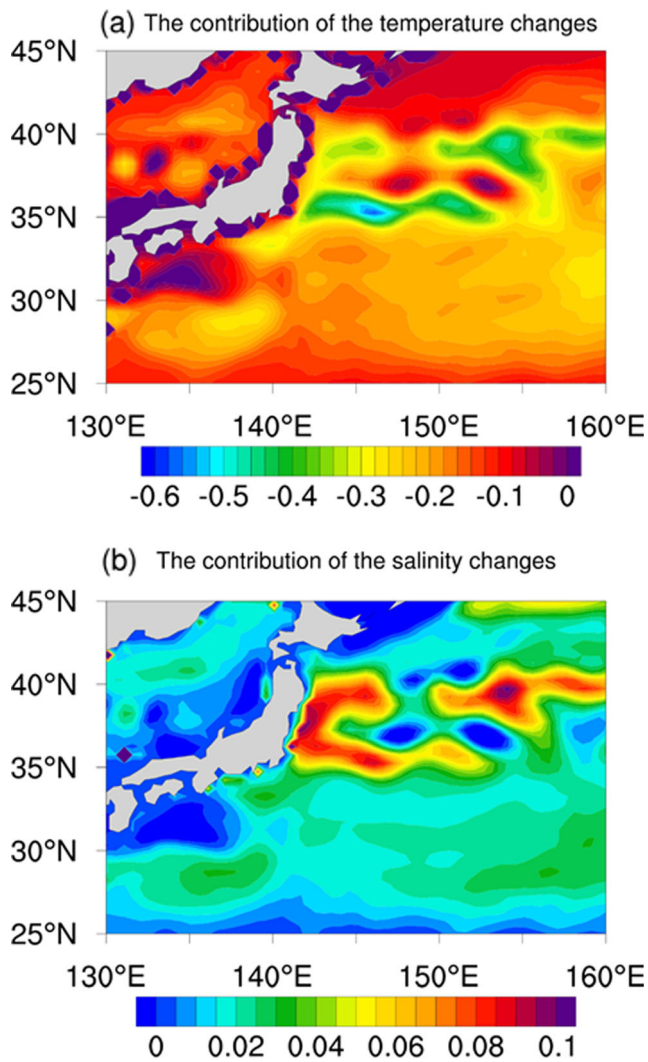
Fig. 10 The contribution of the temperature (**a**) and salinity (**b**) changes to the potential density (unit, g m^{-3}) changes at 200 m
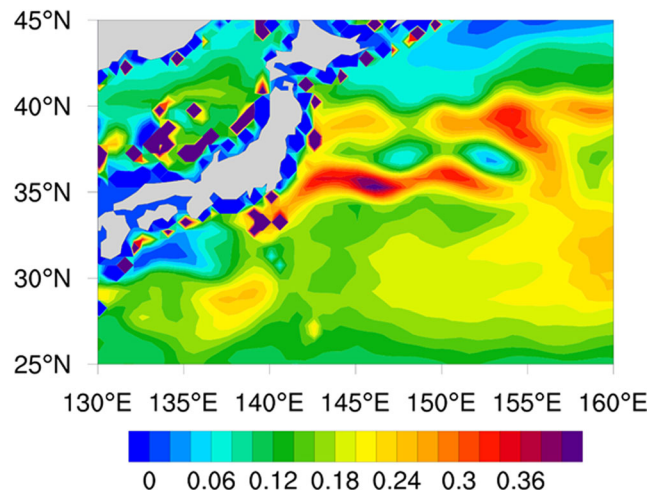

Fig. 11 The difference between the stratification (stratification is computed as the differences between 1000 and 200 m potential density changes) of ensemble historical simulation (H1) and future emission scenarios simulation (R1) (latter minus former); unit, g m^{-3}

temperature changes are the major contributor to the density changes in most regions: the contribution of temperature changes is five times larger around the KE region than that of salinity changes (the contribution of temperature is −0.5 g m^{-3} while the contribution of salinity is only 0.1 g m^{-3}). We also examine the spatial distributions of the stratification changes (Fig. 11), which is remarkably similar to Fig. 10a. This is because the temperature changes in the upper ocean are the main reason that causes changes in potential density around the KE region as mentioned above. In short, the stratification in the SRG region indeed enhances in MIROC4h under global warming condition, which results from the large decrease in upper ocean density mainly induced by temperature changes. According to Liu (1997) and Sun et al. (2013), the enhanced ocean stratification could intensify the strength of the SRG significantly. Thus, the ocean stratification changes indeed contribute to the spin-up of the SRG to some extent.

In the following, we briefly show how the enhanced stratification leads to the strengthening of the SRG. We should point out that the following analysis is qualitative. In fact, it is very difficult for us to quantitatively estimate the effects of the stratification changes on the enhancement of the SRG because the effects of the stratification change are not able to be separated from the effects of the wind change unless a group of twin experiments are performed to exclude the roles of one of them using a climate model. We define the potential vorticity for upper and deeper oceans according to Pedlosky (1987) and Sun et al. (2013) as follows:

$$q_1 = \nabla^2 \psi_1 + F_1(\psi_2 - \psi_1) + \beta y \qquad (5a)$$

$$q_2 = \nabla^2 \psi_2 + F_2(\psi_1 - \psi_2) + \beta y$$
$$F_1 = \frac{f_0^2}{g' H_1}, \ F_2 = \frac{f_0^2}{g' H2} \qquad (5b)$$

where $g' = g(\rho_2 - \rho_1)/\rho_0$ represents the reduced gravity parameter; ρ_1, ρ_2, and ρ_0 indicate the density for the upper ocean, the deeper ocean, and the reference state, respectively. The first term on the right-hand side of Eq. (5) is the relative potential vorticity (RPV); the second term is the thickness potential vorticity (TPV); and the last term is the planetary potential vorticity. Note that only the thickness potential vorticity $F_i(\psi_{3-i} - \psi_i)$ is explicitly connected to stratification. It is worth mentioning that the sign of the TPV in the upper ocean is negative because $\psi_2 - \psi_1$ is negative while F_1 is positive. With the intensification of stratification, F_1 reduces, which will lead to the decrease in the absolute value of the TPV. This means the increase of the TPV, which will lead to the decrease in the RPV if there are no variations in the potential vorticity q_1. Because the SRG is an anticyclone, the sign of the RPV is negative in the SRG region. Hence, the absolute value of the RPV increases, which means that the anticyclonic SRG

strengthens. In this way, the change in ocean stratification contributes to the enhancement of the SRG. Physically, as the stratification strengthens, the momentum transferring from the upper ocean to the deeper ocean will reduce.

In order to verify whether the mechanism mentioned above operates in the MIROC4h model, we plot Fig. 12a, b to show the differences of TPV and RPV at 200 m between historical simulation (H1) and future emission scenarios simulation (R1) (latter minus former). Because the differences of TPV ranging from surface to 400 m show similar results, for simplicity, we only indicate the results for 200 m here. To calculate the RPV and TPV, we use current velocities at 200 and 1000 m to calculate the stream functions ψ_1 and ψ_2 and then calculate RPVs $\nabla^2 \psi_1$ for upper ocean and $\nabla^2 \psi_2$ for deeper ocean. Besides, we use density difference between 200 and 1000 m to compute the reduced gravity and the TPV. As shown in Fig. 12a, b, the RPV changed largely in the region where
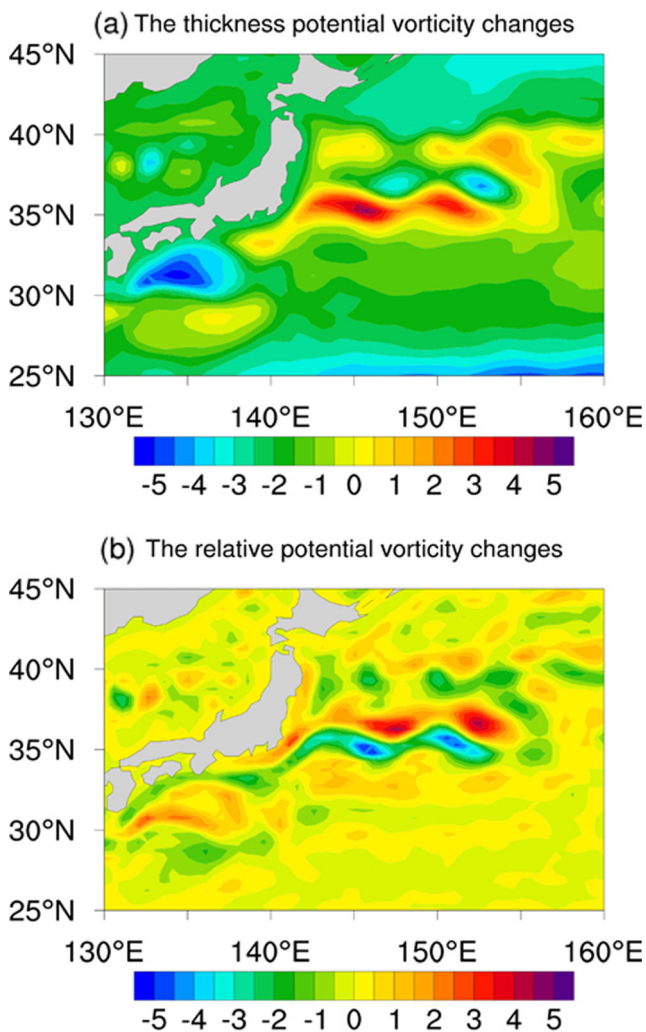

Fig. 12 a The thickness potential vorticity changes at 200 m between historical simulation (H1) and future emission scenarios simulation (R1) (latter minus former). **b** The relative potential vorticity changes at 200 m between historical simulation (H1) and future emission scenarios simulation (R1) (latter minus former); unit, $10^{-6}\ \mathrm{s}^{-1}$

TPV intensified obviously and it also corresponded to the region where ocean stratification enhanced significantly if comparing Fig. 12a, b with Fig. 11. One point we should mention, the wind stress forcing changes can also affect the TPV by changing the stream function ψ_1. In other words, the effects of wind and ocean stratification changes are not linearly additive and cannot be separated in MIROC4h in this study. The relative importance of the wind stress changes and stratification changes needs to be further investigated.

Besides affecting the TPV, the strengthened ocean stratification could enhance the ocean baroclinic instability by increasing the vertical shear in the KE system, resulting in a higher level of regional the eddy kinetic energy (EKE). Many theoretical and modeling studies in the past have indicated that the eddy momentum flux forcing can feedback to modify the time-mean circulation (e.g., Greatbatch et al. 2010; Qiu and Chen 2010; Qiu et al. 2015). Qiu et al. (2015) confirmed that the increase of EKE level in the downstream KE region (33°–37°N, 150°–170°E) would intensify the SRG. Following Qiu et al. (2015), we calculate the EKE changes in the downstream KE region, and the results show that the EKE increases about 10 % in three simulations under warming scene. Thus, the increased EKE caused by the strengthened stratification also contributes to the intensification of the SRG on some level. It should be noted that most climate models use coarse-resolution ocean models (1°×1° or coarser) in CMIP5 experiments. The coarse-resolution ocean model does not allow ocean baroclinic instability to fully develop and may not well characterize the process that eddy momentum flux forcing feedback to modify the time-mean circulation. This re-emphasizes that using a high-resolution ocean model is very important when we focus on the KE system studies.

By the combined effects of wind stress and stratification changes, the SRG intensifies under global warming. Then the enhancement of the SRG results in the large acceleration of the KE. Finally, both the KE and its SRG intensify under global warming condition.

6 Summary and discussion

The KE system is an important part of western boundary current. The variations of the KE and its SRG have a significant impact not only on the local climate but also on the global climate through air-sea interaction. It is an interesting issue to investigate the effects of global warming to the KE system and the mechanism.

In the present study, we use the datasets of a new high-resolution climate model MIROC4h. Results show that the KE front and its SRG could be well represented in the MIROC4h model. MIROC4h can also capture the feature of the spatial and temporal structures of the KE's low-frequency

variations. To our knowledge, no previous studies focusing on the KE's low-frequency variations use climate models because most ocean models used in the climate models are coarse-resolution models and the KE cannot be simulated well in these models. As far as we know, MIROC4h is probably the only climate model used in CMIP5, which is able to simulate the low-frequency variations of KE system because of its relative high resolution compared with other climate models. Therefore, we use MIROC4h to investigate how the KE system will evolve under global warming and reveal the mechanisms.

Comparing three-ensemble historical simulations with three subsequent future emission scenarios simulations, it turns out that the KE intensifies eastward transport and its SRG enhances in all three future emission scenarios simulations. We examine the difference in the stream function for the upper ocean induced by warming and find that there exist negative anomalies in the most subtropical region, which confirm that the whole of the subtropical gyre does not spin-up under global warming condition. This implies that intensification of the KE system is maybe due to the changes of local surroundings rather than remote surroundings. Therefore, we investigate the changes of local wind stress and stratification. It turns out that the wind stress changes and ocean stratification changes both contribute to the enhancement of the KE system. Specifically, the wind stress changes increase the upper ocean momentum in the SRG region. Meanwhile, the increased stratifications hinder the momentum transfer from the upper ocean to the deeper ocean. Besides, the strengthened ocean stratification could enhance the EKE in the downstream KE region which can feedback to intensify the SRG. As a result, the SRG intensifies under global warming condition. Then spin-up of the SRG results in large acceleration of the KE. Eventually, the KE system intensifies under warming scene.

In this study, we qualitatively illustrate that wind stress changes and ocean stratification changes both contribute to the enhancement of the KE system. However, it is very difficult for us to quantitatively estimate the effects of the wind stress changes or the stratification changes on the intensification of the KE and its SRG because the effects of them are not linearly additive and cannot be separated through analysis of climate model data in this study. In order to quantify the relative importance of the wind stress changes and stratification changes, a group of twin experiments should be performed to exclude the roles of one of them using a climate model. This is an important aspect of our study in the future.

References

Beliakova NY (1998) Generation and maintenance of recirculation by Gulf Stream instabilities. Ph.D. thesis, Massachusetts Institute of Technology/Woods Hole Oceanographic Institute Joint Program, 224 pp

Berloff PS (2005) On rectification of randomly forced flows. J Mar Res 63(3):497–527

Capotondi A, Alexander MA, Bond NA et al (2012) Enhanced upper ocean stratification with climate change in the CMIP3 models. J Geophys Res 117:C04031

Ceballos LI, Lorenzo ED, Hoyos CD et al (2009) North Pacific gyre oscillation synchronizes climate fluctuations in the eastern and western boundary systems. J Clim 22(19):5163–5174

Cessi P (1988) A stratified model of the inertial recirculation. J Phys Oceanogr 18(4):662–682

Chang KI, Ghil M, Ide K et al (2001) Transition to aperiodic variability in a wind-driven double-gyre circulation model. J Phys Oceanogr 31: 1260–1286

Choi BH, Kim DH, Kim JW (2002) Regional responses of climate in the Northwestern Pacific Ocean to gradual global warming for a CO_2 quadrupling. J Meteorol Soc Jpn 80(6):1427–1442

Clarke L, Edmonds J, Jacoby H, Pitcher H, Reilly J, Richels R (2007) Scenarios of greenhouse gas emissions and atmospheric concentrations. US Department of Energy Publications 6

Cravatte S, Delcroix T, Zhang D et al (2009) Observed freshening and warming of the western Pacific warm pool. Clim Dyn 33:565–589

Deser C, Phillips S, Alexander MA (2010) Twentieth century tropical sea surface temperature trends revisited. Geophys Res Lett 37(10): L10701

Dijkstra HA (2000) Nonlinear physical oceanography. Kluwer Academic, 480 pp

Dijkstra HA, Ghil G (2005) Low-frequency variability of the large scale ocean circulation: a dynamical approach. Rev Geophys 43(3): RG302

Frankignoul C, Sennéchael N, Kwon YO et al (2011) Influence of the meridional shifts of the Kuroshio and the Oyashio extensions on the atmospheric circulation. J Clim 24(3):762–776

Greatbatch RJ, Zhai XM, Kolmann JD, Czeschel L (2010) Ocean eddy momentum fluxes at the latitudes of the Gulf Stream and the Kuroshio extensions as revealed by satellite data. Ocean Dyn 60: 617–628

Guan B, Nigam S (2008) Pacific sea surface temperatures in the twentieth century: an evolution-centric analysis of variability and trend. J Clim 21(12):2790–2809

Hasumi H (2006) CCSR Ocean Component Model (COCO) version 4.0. CCSR Report 25: 103 pp

Houghton JT, Ding Y, Griggs DJ et al (2001) Climate change 2001: the scientific basis. Cambridge University Press, Cambridge

Jayne SR, Hogg NG (1999) On recirculation forced by an unstable jet. J Phys Oceanogr 29:2711–2718

Jayne SR, Hogg NG, Rizzoli P (1996) Recirculation gyres forced by a beta-plane jet. J Phys Oceanogr 26:492–504

K-1 Model Developers (2004) In: Hasumi H, Emori S (eds) K-1 coupled GCM (MIROC) description, K-1 Tech. Rep., 1. Center for Climate System Research, the University of Tokyo, Tokyo, 34 pp

Kelly KA, Small RJ et al (2010) Western boundary currents and frontal air-sea interaction: gulf stream and Kuroshio Extension. J Clim 23(21):5644–5667

Komuro A, Ono R, Oda T (2012) Numerical simulation for production of O and N radicals in an atmospheric-pressure streamer discharge. J Phys D Appl Phys 45(26):265201

Kwon YO, Alexander MA, Bond NA et al (2010) Role of the Gulf Stream and Kuroshio–Oyashio systems in large-scale atmosphere–ocean interaction: a review. J Clim 23(12):3249–3281

Liu ZY (1997) The influence of stratification on the inertial recirculation. J Phys Oceanogr 27:926–940

Marshall D, Marshall J (1992) Zonal penetration scale of midlatitude oceanic jets. J Phys Oceanogr 22(9):1018–1032

Marshall J, Nurser A (1986) Steady, free circulation in a stratified quasi-geostrophic ocean. J Phys Oceanogr 16:1799–1813

Miller AJ, Cayan DR, White WB (1998) A westward-intensified decadal change in the North Pacific thermocline and gyre-scale circulation. J Clim 11(12):3112–3127

Moss RH, Babiker M, Brinkman S et al (2008) Towards new scenarios for analysis of emissions, climate change, impacts, and response strategies. IPCC Expert Meeting Report on New Scenarios. Intergovernmental Panel on Climate Change, Noordwijkerhout

Moss RH, Edmonds JA, Hibbard KA et al (2010) The next generation of scenarios for climate change research and assessment. Nature 463(7282):747–756

Pedlosky J (1987) Geophysical fluid dynamics. 2nd ed. Springer, 710 pp

Pierini S (2006) A Kuroshio Extension system model study: decadal chaotic self-sustained oscillations. J Phys Oceanogr 36:1605–1625

Pierini S (2015) A comparative analysis of Kuroshio Extension indices from a modeling perspective. J Clim 28(14):5873–5881

Pierini S, Dijkstra HD, Riccio A (2009) A nonlinear theory of the Kuroshio extension bimodality. J Phys Oceanogr 39:2212–2229

Qiu B (2002) The Kuroshio Extension system: its large-scale variability and role in the midlatitude ocean-atmosphere interaction. J Oceanogr 58(1):57–75

Qiu B (2003) Kuroshio Extension variability and forcing of the Pacific decadal oscillations: responses and potential feedback. J Phys Oceanogr 33(12):2465–2482

Qiu B, Chen S (2005) Variability of the Kuroshio Extension jet, recirculation gyre, and mesoscale eddies on decadal time scales. J Phys Oceanogr 35(11):2090–2103

Qiu B, Chen S (2010) Eddy-mean flow interaction in the decadally modulating Kuroshio Extension system. Deep-Sea Res II Top Stud Oceanogr 57(13):1098–1110

Qiu B, Miao W (2000) Kuroshio path variations south of Japan: bimodality as a self-sustained internal oscillation. J Phys Oceanogr 30:2124–2137

Qiu B, Chen S, Hacker P, Hogg NG, Jayne SR, Sasaki H (2008) The Kuroshio Extension northern recirculation gyre: profiling float measurements and forcing mechanism. J Phys Oceanogr 38(8):3112–3127

Qiu B, Chen S, Schneider N, Taguchi B (2014) A coupled decadal prediction of the dynamic state of the Kuroshio Extension system. J Clim 27(4):1751–1764

Qiu B, Chen S, Wu LX, Shinichiro K (2015) Wind- versus eddy-forced regional sea level trends and variability in the North Pacific Ocean. J Clim 28:1561–1577

Sakamoto TT, Hasumi H, Ishii M, Emori S, Suzuki T, Nishimura T, Sumi A (2005) Responses of the Kuroshio and the Kuroshio Extension to global warming in a high-resolution climate model. Geophys Res Lett 32(14):L14617

Sakamoto TT, Komuro Y, Nishimura T et al (2012) MIROC4h-a new high-resolution atmosphere-ocean coupled general circulation model. J Meteorol Soc Jpn 90(3):325–359

Sasaki YN, Minobe S, Schneider N (2013) Decadal response of the Kuroshio Extension jet to Rossby Waves: observation and thin-jet theory. J Phys Oceanogr 43(2):442–456

Schneider N, Miller AJ, Pierce DW (2002) Anatomy of North Pacific decadal variability. J Clim 15(6):586–605

Sun ST, Wu LX, Qiu B (2013) Response of the inertial recirculation to intensified stratification in a Two-Layer Quasi-geostrophic Ocean Circulation Model. J Phys Oceanogr 43(7):1254–1269

Susan S, Qin D, Martin M (2007) Climate change 2007-the physical science basis: working group I contribution to the fourth assessment report of the IPCC (Vol. 4). Cambridge University Press, Cambridge

Taguchi B, Xie SP, Mitsudera H, Kubokawa A (2005) Response of the Kuroshio Extension to Rossby Waves associated with the 1970s climate regime shift in a high-resolution ocean model. J Clim 18:2979–2995

Taguchi B, Xie SP, Schneider N, Nonaka M, Sasaki H, Sasai Y (2007) Decadal variability of the Kuroshio Extension: observations and an eddy-resolving model hindcast. J Clim 20(11):2357–2377

Taguchi B, Qiu B, Nonaka M, Sasaki H, Xie SP, Schneider N (2010) Decadal variability of the Kuroshio Extension: mesoscale eddies and recirculations. Ocean Dyn 60(3):673–691

Takata K, Emori S, Watanabe T (2003) Development of the minimal advanced treatments of surface interaction and runoff (MATSIRO). Global Planet Change 38:209–222

Taylor KE, Stouffer RJ, Meehl GA (2012) An overview of CMIP5 and the experiment design. Bull Am Meteorol Soc 93(4):485–498

Waterman SN, Jayne SR (2009) Eddy–mean flow interaction in the along-stream development of a western boundary current jet: an idealized model study. J Phys Oceanogr 41:681–707